Space Object Material Determination from Polarized Light Curves

Andrew D. Dianetti* and John L. Crassidis†
University at Buffalo, State University of New York, Amherst, New York, 14260-4400

Surface material identification of resident space objects is demonstrated using polarized monochromatic light curves. The specular reflection of unpolarized light off a flat surface creates a reflection that is partially polarized. This polarization depends on the index of refraction and the extinction coefficient of the reflecting material. Thus, the degree of polarization contains information about the surface material that is not contained in the unpolarized light curve. A polarized bidirectional reflectance distribution function is developed to generate polarized light curves. Surface material observability is analyzed. Multiple-model adaptive estimation is used to identify the surface material from a bank of candidate materials when specular reflection occurs. Results indicate that the polarized light curves can accurately determine material properties os a resident space object.

I. Introduction

A key area to improved space situational awareness (SSA) is being able to characterize attributes of resident space objects (RSOs) beyond just an object's orbit and ballistic coefficient. Of specific interest are the object's shape, attitude and surface properties, including surface materials. All of these attributes can influence an object's orbit through the effects of drag or solar radiation pressure. For large objects in low-Earth orbit (LEO), methods such as resolved imaging or radar cross-sectioning can be used to provide information about an object's shape or attitude. However, objects in higher orbits, such as geosynchronous orbit (GEO), are too distant for these methods to be effective.

Light curves, or the temporal history of an object's brightness, have been used to estimate an object's shape and attitude. Attitude has been shown to be observable from light curves [1]. This work also demonstrates the observability of surface reflectance parameters, but is limited to properties of the reflectance models and not surface materials. Attitude estimation has been demonstrated from light curve data, assuming that shape and surface reflectance properties are well-known [2]. Shape estimation has been demonstrated in conjunction with attitude estimation by employing multiple-model adaptive estimation (MMAE) [3]. Shape, attitude profile and surface reflectance parameter estimation have been demonstrated using a multiple-hypothesis approach [4]. This approach simply uses three common attitude profiles, and surface parameters are estimated as part of each hypothesis, not as filtered states. Simultaneous orbit, attitude and surface parameter estimation from angles and light curve data has been demonstrated, however, it is seen that it is often difficult to simultaneously estimate surface parameters, as the filters suffer from information dilution [5]. Simultaneous orbit, attitude, area and mass estimation from angles and light curve data has also been demonstrated [6]. In this work, the coupled albedo-area was estimated from photometric data and the area-to-mass ratio from astrometric data. This allowed for the object's mass to be determined. Knowledge of an object's surface materials not only allows for better categorization of an object, but can also allow for more accurate surface reflectance determination. Since surface reflectance depends on the material, knowledge of the surface materials can provide more information about their reflectance. This could lead to better modeling of solar radiation pressure, which would increase the accuracy of orbit propagation, especially for GEO objects. Multispectral light curves are one method by which surface material abundances can be estimated [7]. In this paper, polarized light curves will be shown to be useful for surface material estimation.

Light curves are typically modeled using a bidirectional reflectance distribution function (BRDF). To date, none of the aforementioned estimation efforts have considered the polarization of the light, and except for [7] and [4], have used only monochromatic light curves. Reference [8] models polarized light curves in three bands for a spacecraft and debris object in LEO. However, no attempts to estimate object attributes are performed in this work.

Polarized light curves are of interest for SSA applications because specular reflections of unpolarized light off a surface are polarized, and this polarization depends on the reflecting material's index of refraction and extinction

*Graduate Student, Department of Mechanical & Aerospace Engineering. Email: andrewdi@buffalo.edu. Student Member AIAA.
†Samuel P. Capen Chair Professor, Department of Mechanical & Aerospace Engineering. Email: johnc@buffalo.edu. Fellow AIAA.

coefficient [9]. Thus, the polarization of the light curve contains information about the object's surface materials. This provides more information over simply using the unpolarized light curve, in both the monochromatic and multispectral case. It is shown in this paper that a monochromatic polarized light curve can be used for surface material estimation, which is not possible with an unpolarized monochromatic light curve. When combined with multispectral imaging, this technique could become more powerful and further increase the observability of surface materials.

In this paper, a polarized bidirectional reflectance distribution function (pBRDF) is described. Then, light curves are simulated from the pBRDF. The direct observability of material properties is evaluated. While it is shown that direct observability of material properties does not exist, an MMAE approach is demonstrated to effectively estimate the surface material of a simulated space object.

II. Bidirectional Reflectance Distribution Functions

In this section, an overview of BRDF models will be given. First, an unpolarized, scalar BRDF model will be described. Then, an overview of the Stokes vector and Mueller matrix representations will be given, and the scalar BRDF model will be extended to a polarized model.

A. Unpolarized BRDF Model

The BRDF model described in this section is that of [10], which is also described in [1]. The apparent magnitude, m_{app}, is computed using the BRDF model and a shape model. The reflection geometry for a single facet is shown in Fig. 1. Each facet has a set of three basis vectors ($\boldsymbol{u}_n^B$, $\boldsymbol{u}_u^B$, $\boldsymbol{u}_v^B$). The unit vector $\boldsymbol{u}_n^B$ points in the direction of the

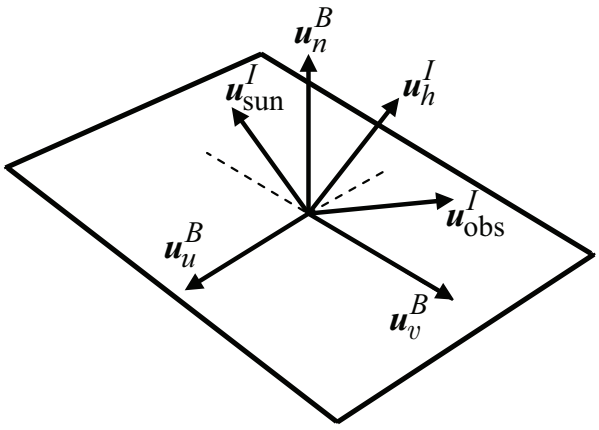

Fig. 1 Facet reflection geometry.

outward normal of the facet, and the vectors $\boldsymbol{u}_u^B$ and $\boldsymbol{u}_v^B$ are in the plane of the facet. In this analysis, the object is assumed to be a rigid body so that the unit vectors $\boldsymbol{u}_n^B$, $\boldsymbol{u}_u^B$ and $\boldsymbol{u}_v^B$ do not change since they are expressed in the body frame. The vector $\boldsymbol{u}_h^I$ is the normalized half vector between $\boldsymbol{u}_{\text{sun}}^I$, the unit vector to the Sun, and $\boldsymbol{u}_{\text{obs}}^I$, the unit vector to the observer. The observation vector is usually given in body coordinates with $\boldsymbol{u}_{\text{obs}}^B = A(\boldsymbol{q})\boldsymbol{u}_{\text{obs}}^I$, where $A(\boldsymbol{q})$ is the inertial-to-body attitude matrix, expressed using quaternions [11].

The BRDF at any point on the surface is a function of two directions, the direction from which the light source originates and the direction from which the scattered light leaves the surface. The BRDF is decomposed into a specular component and a diffuse component. The two terms sum to give the total BRDF:

$$\rho_{\text{total},i} = \rho_{\text{spec},i} + \rho_{\text{diff},i} \tag{1}$$

The diffuse component represents light that is scattered equally in all directions (Lambertian) and the specular component represents light that is concentrated about some direction (mirror-like). Reference [10] develops a model for continuous arbitrary surfaces but simplifies it for flat surfaces. This simplified model is employed in this work as the shape models are considered to consist of a finite number of flat facets. Therefore the total observed brightness of an object becomes the sum of the contribution from each facet.

Under the flat facet assumption, the specular term of the BRDF becomes

$$\rho_{\text{spec},\,i} = \frac{\sqrt{(n_u+1)\,(n_v+1)}}{8\pi} \frac{\left(\boldsymbol{u}^I_{n,\,i}\cdot\boldsymbol{u}^I_h\right)\left\{\dfrac{n_u(\boldsymbol{u}^I_h\cdot\boldsymbol{u}^I_{u,\,i})^2+n_v(\boldsymbol{u}^I_h\cdot\boldsymbol{u}^I_{v,\,i})^2}{\left(1-\left[\boldsymbol{u}^I_{n,i}\cdot\boldsymbol{u}_{h,j}\right]^2\right)}\right\}}{\boldsymbol{u}^I_{n,\,i}\cdot\boldsymbol{u}^I_{\text{sun}}+\boldsymbol{u}^I_{n,\,i}\cdot\boldsymbol{u}^I_{\text{obs}}-(\boldsymbol{u}^I_{n,\,i}\cdot\boldsymbol{u}^I_{\text{sun}})(\boldsymbol{u}^I_{n,\,i}\cdot\boldsymbol{u}^I_{\text{obs}})} F_{\text{reflect},\,i} \tag{2}$$

where the Fresnel reflectance is given by

$$F_{\text{reflect},i} = R_{\text{spec},i} + (1-R_{\text{spec},i})(1-\boldsymbol{u}^I_{\text{sun}}\cdot\boldsymbol{u}^I_{h,i})^5 \tag{3}$$

If the surface was perfectly smooth, all of the Fresnel reflectance would be directed along the reflectance angle, expressed in body coordinates as

$$\boldsymbol{u}^B_{\text{reflect}} = \boldsymbol{u}^B_{\text{sun}} - 2(\boldsymbol{u}^B_{\text{sun}}\cdot\boldsymbol{u}^B_n)\boldsymbol{u}^B_n \tag{4}$$

where $\boldsymbol{u}^B_{\text{sun}}$ is the Sun vector in body coordinates. However, real materials have some level of surface roughness, which results in many small surface normals that are oriented in different directions. Therefore, the specular reflectance can be thought of as a cone distributed around the specular reflection direction given in Eq. (4), with the distribution (in the local u and v directions) defined by the terms n_u and n_v. The diffuse term of the BRDF is given by

$$\rho_{\text{diff},i} = \left(\frac{28R_{\text{diff},i}}{23\pi}\right)(1-R_{\text{spec},i})\left[1-\left(1-\frac{\boldsymbol{u}^I_{n,i}\cdot\boldsymbol{u}^I_{\text{sun}}}{2}\right)^5\right]\left[1-\left(1-\frac{\boldsymbol{u}^I_{n,i}\cdot\boldsymbol{u}^I_{\text{obs}}}{2}\right)^5\right] \tag{5}$$

The apparent magnitude of the object is the result of sunlight reflecting off of its surfaces along the line-of-sight to an observer. First, the fraction of visible sunlight that strikes an object is computed by

$$F_{\text{sun},i} = C_{\text{sun,vis}}\rho_{\text{total},i}(\boldsymbol{u}^I_{n,i}\cdot\boldsymbol{u}^I_{\text{sun}}) \tag{6}$$

where $C_{\text{sun,vis}} = 455$ W/m^2 is the power per square meter impinging on a given object due to visible light striking the surface. If either the angle between the surface normal and the observer's direction or the angle between the surface normal and the Sun direction is greater than $\pi/2$ then there is no light reflected toward the observer. If this is the case then the fraction of visible light is set to $F_{\text{sun},i} = 0$.

The fraction of sunlight that strikes a surface that is reflected is given by

$$F_{\text{obs},i} = \frac{F_{\text{sun},i}A_{\text{facet},i}(\boldsymbol{u}^I_{n,i}\cdot\boldsymbol{u}^I_{\text{obs}})}{d^2} \tag{7}$$

where d is the distance from the observer to the object and $A_{\text{facet},i}$ is the area of the facet. The reflected light is now used to compute the apparent brightness magnitude, which is measured by an observer through

$$m_{\text{app}} = -26.7 - 2.5\log_{10}\left|\sum_{i=1}^{N}\frac{F_{\text{obs},i}}{C_{\text{sun,vis}}}\right| \tag{8}$$

where -26.7 is the apparent magnitude of the Sun, and N is the total number of facets. It is important to note that m_{app} is defined across a certain wavelength range − in this case, the entire visible spectrum. If a multispectral BRDF were to be considered, $m_{\text{app},\lambda}$ would be defined for each band λ, and $C_{\text{sun,vis},\lambda}$ would then be the Watts per square meter of sunlight in the wavelength range for that band. A vector of measurements for each wavelength range λ would then be available, as opposed to a single scalar.

B. Polarized Light Representations

While the scalar m_{app} gives the total intensity of the reflected light, it does not contain information about the light's polarization. However, the Fresnel reflectance of unpolarized light (such as sunlight) will be polarized so long as the vectors $\boldsymbol{u}^I_h$ and $\boldsymbol{u}^I_n$ are not aligned. One common example of this phenomenon can be observed by looking at the

surface of a body of water or a metal roof while wearing polarized sunglasses. Since many surfaces of space objects are relatively flat, they will produce polarized Fresnel reflectance components. Measures of this polarization will provide additional information beyond the scalar magnitude.

Polarized light is most often described using the Stokes vector notation. The Stokes vector is composed of the Stokes parameters, which are defined in terms of the polarization ellipse. Elliptical polarization is the most general form of polarized light. It can be resolved into two linearly polarized waves offset by $\pi/2$ radians (phase quadrature). The projection of these waves on a plane perpendicular to the light's direction of travel will form an ellipse. Figure 2 shows the polarization ellipse. The polarization ellipse can be expressed mathematically as [9]

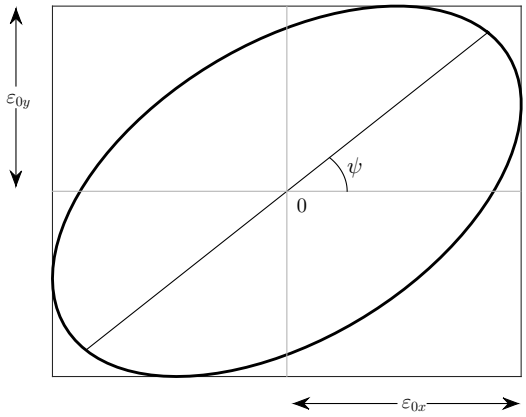

Fig. 2 Polarization ellipse.

$$\frac{\varepsilon_{\mathrm{x}}^2}{\varepsilon_{0\mathrm{x}}^2} + \frac{\varepsilon_{\mathrm{y}}^2}{\varepsilon_{0\mathrm{y}}^2} + \frac{-2\varepsilon_{\mathrm{x}}\varepsilon_{\mathrm{y}}}{\varepsilon_{0\mathrm{x}}\varepsilon_{0\mathrm{y}}}\cos\phi = \sin^2\phi \tag{9}$$

The polarization angle, denoted as ψ in Fig. 2, is computed as [9]

$$\tan 2\psi = \frac{2\varepsilon_{0\mathrm{x}}\varepsilon_{0\mathrm{y}}\cos\phi}{\varepsilon_{0\mathrm{x}}^2 - \varepsilon_{0\mathrm{y}}^2} \tag{10}$$

Stokes showed that if the time averages of ε_{x} and ε_{y} are taken, that Eq. (9) becomes

$$(\varepsilon_{0\mathrm{x}}^2 + \varepsilon_{0\mathrm{y}}^2)^2 = (\varepsilon_{0\mathrm{x}}^2 - \varepsilon_{0\mathrm{y}}^2)^2 + (2\varepsilon_{0\mathrm{x}}\varepsilon_{0\mathrm{y}}\cos\phi)^2 + (2\varepsilon_{0\mathrm{x}}\varepsilon_{0\mathrm{y}}\sin\phi)^2 \tag{11}$$

From this, the Stokes parameters are defined as [9]

$$S_0 = \varepsilon_{0\mathrm{x}}^2 + \varepsilon_{0\mathrm{y}}^2 \tag{12a}$$

$$S_1 = \varepsilon_{0\mathrm{x}}^2 - \varepsilon_{0\mathrm{y}}^2 \tag{12b}$$

$$S_2 = 2\varepsilon_{0\mathrm{x}}\varepsilon_{0\mathrm{y}}\cos\phi \tag{12c}$$

$$S_3 = 2\varepsilon_{0\mathrm{x}}\varepsilon_{0\mathrm{y}}\sin\phi \tag{12d}$$

It is important to note that these parameters are real quantities that have units of intensity or energy in a beam. S_0 describes the total energy in a beam, S_1 describes the amount of linear horizontal or vertical polarization, S_2 describes the amount of $\pm 45°$ linear polarization, and S_3 describes the amount of right- or left-handed circular polarization [9]. Note that Eq. (11) describes fully polarized light, and thus if the light is partially polarized, this will increase the S_0 term such that $S_0^2 > S_1^2 + S_2^2 + S_3^2$. Thus, for describing the generalized case of partially polarized light, the Stokes parameters are not redundant. The Stokes vector $\boldsymbol{S}$ is formed from the Stokes parameters:

$$\boldsymbol{S} = \begin{bmatrix} S_0 \\ S_1 \\ S_2 \\ S_3 \end{bmatrix} \tag{13}$$

Note that if $\varepsilon_0^2 \equiv \varepsilon_{0\mathrm{x}}^2 + \varepsilon_{0\mathrm{y}}^2$, then $S_0 = \varepsilon_0^2$, and the Stokes vector can be written as

$$\boldsymbol{S} = \varepsilon_0^2 \hat{\boldsymbol{S}} \tag{14}$$

where

$$\hat{\boldsymbol{S}} \equiv \begin{bmatrix} 1 \\ S_1/S_0 \\ S_2/S_0 \\ S_3/S_0 \end{bmatrix} \tag{15}$$

Here, $\hat{\boldsymbol{S}}$ contains the polarization state of the light beam without containing its total intensity. It is also common to refer to this quantity as the Stokes vector [9]. In this paper, the terms $\boldsymbol{S}$ and $\hat{\boldsymbol{S}}$ will be used to avoid confusion. The $\hat{\boldsymbol{S}}$ vector can be used to describe a number of important polarization states. Randomly polarized (or "unpolarized") light has $\hat{\boldsymbol{S}} = [1 \;\; 0 \;\; 0 \;\; 0]^T$. Linear horizontal polarization has $\hat{\boldsymbol{S}} = [1 \;\; 1 \;\; 0 \;\; 0]^T$ and linear vertical polarization has $\hat{\boldsymbol{S}} = [1 \;\; -1 \;\; 0 \;\; 0]^T$. Linear +45° polarization has $\hat{\boldsymbol{S}} = [1 \;\; 0 \;\; 1 \;\; 0]^T$ and linear −45° polarization has $\hat{\boldsymbol{S}} = [1 \;\; 0 \;\; -1 \;\; 0]^T$. Right-handed circular polarization has $\hat{\boldsymbol{S}} = [1 \;\; 0 \;\; 0 \;\; 1]^T$ and left-handed circular polarization has $\hat{\boldsymbol{S}} = [1 \;\; 0 \;\; 0 \;\; -1]^T$.

C. Modeling Polarized Reflections

Given the Stokes vector representation of polarized light, a method by which to compute the polarized reflection of a light beam must be implemented. The Mueller matrix, M, allows the Stokes vector of an incoming light beam, $\boldsymbol{S}_{\mathrm{in}}$, to the Stokes vector of a transmitted or reflected light beam, $\boldsymbol{S}_{\mathrm{out}}$:

$$\boldsymbol{S}_{\mathrm{out}} = M\boldsymbol{S}_{\mathrm{in}} \tag{16}$$

Mueller matrices can be defined for either transmission through a medium or reflection off a surface. The Mueller matrix for polarimetric Fresnel reflection is given by [9]

$$M_R = \frac{1}{2}\begin{bmatrix} R_s + R_p & R_s - R_p^2 & 0 & 0 \\ R_s - R_p & R_s + R_p & 0 & 0 \\ 0 & 0 & 2\mathrm{Re}(r_s r_p^*) & 2\mathrm{Im}(r_s r_p^*) \\ 0 & 0 & -2\mathrm{Im}(r_s r_p^*) & 2\mathrm{Re}(r_s r_p^*) \end{bmatrix} \tag{17}$$

where $r_s = \sqrt{R_s}$, $r_p = \sqrt{R_p}$, Re and Im refer to the real imaginary parts and the superscript * denotes the complex conjugate. R_s is the Fresnel reflectance coefficient for radiation perpendicular to the plane of incident flux and R_p is the Fresnel reflectance coefficient for radiation parallel to the plane of incident flux.

Since sunlight is randomly polarized, it has a Stokes vector of $\boldsymbol{S}_{\mathrm{in}} = [1 \;\; 0 \;\; 0 \;\; 0]^T$. Thus, the Stokes vector of the Fresnel reflection is

$$\boldsymbol{S}_F = \begin{bmatrix} R_s + R_p \\ R_s - R_p \\ 0 \\ 0 \end{bmatrix} \tag{18}$$

From this, it is seen that Fresnel reflectance of randomly polarized light has linear horizontal or vertical polarization, but no ±45° or circular polarization. Thus, in the case of reflected sunlight, the measurements are the S_0 and S_1 components of the reflected light. Note that S_0 is the total intensity, as is used in unpolarized light curve analysis. Polarimetric observations add a second measurement, the S_1 component.

D. Polarized BRDF Model

The BRDF model presented in the earlier section is now extended to the polarized case. The polarized s- and p-components of the Fresnel reflection must be computed. R_s and R_p can be computed as [9]

$$R_s = \left| \frac{(n^2 - \sin^2\theta_i)^{1/2} - \cos\theta_i}{(n^2 - \sin^2\theta_i)^{1/2} + \cos\theta_i} \right|^2 \tag{19a}$$

$$R_p = \left| \frac{n^2 \cos\theta_i - (n^2 - \sin^2\theta_i)^{1/2}}{n^2 \cos\theta_i + (n^2 - \sin^2\theta_i)^{1/2}} \right|^2 \tag{19b}$$

where $n \equiv n_2/n_1$ is the relative index of refraction of the reflected medium to the medium of the incident beam and θ_i is the angle of incidence. Note that specular reflection is reflected along the angle $\theta_r = \theta_i$ in the plane of incidence. If the surface is modeled as a distribution of microfacets, only the microfacets that are oriented such that $\boldsymbol{u}_n = \boldsymbol{u}_h$ will have specular reflection visible by the observer. The terms in Eq. (2) that multiply F_{reflect} define the distribution of facets oriented in this direction. Thus, it is seen that the degree of polarization is independent from the orientation of the facet. For given locations of the observer, reflecting body, and light source, the angle θ_i is replaced by θ, or the angle between the object-Sun and object-observer vectors. If it is assumed that the reflecting material is in a vacuum, $n_1 = 0$ and thus $n = n_2$. This formulation is valid for complex indices of refraction [8] of the form

$$n = m + ik \tag{20}$$

where m is the index of refraction and k is the extinction coefficient. For dielectric materials, $k = 0$ and thus n is real. For conductors (such as metals), k is nonzero, and thus n is complex. Equation (19) can be expanded to [12]

$$R_s = \frac{a^2 + b^2 - 2a\cos\theta + \cos^2\theta}{a^2 + b^2 + 2a\cos\theta + \cos^2\theta} \tag{21a}$$

$$R_p = R_s \frac{a^2 + b^2 - 2a\sin\theta\tan\theta + \sin^2\theta\tan^2\theta}{a^2 + b^2 + 2a\sin\theta\tan\theta + \sin^2\theta\tan^2\theta} \tag{21b}$$

where

$$a^2 = \frac{1}{2}\left\{ \sqrt{(m^2 - k^2 - \sin^2\theta)^2 + 4m^2k^2} + m^2 - k^2 - \sin^2\theta \right\} \tag{22a}$$

$$b^2 = \frac{1}{2}\left\{ \sqrt{(m^2 - k^2 - \sin^2\theta)^2 + 4m^2k^2} - (m^2 - k^2 - \sin^2\theta \right\} \tag{22b}$$

R_s and R_p are the components of the Fresnel reflection in the planes perpendicular and parallel to the plane of the incident flux, respectively. The unpolarized Fresnel reflectance is simply the average $F_{\text{reflect}} = 1/2(R_s + R_p)$. This formulation could be used in place of Eq. (3) if m and k are known for the material. However, m and k will vary with wavelength, and these values must be known for each wavelength being considered, e.g. m_λ and k_λ. In practice, these are often unknown and only a single value at the middle of the visible spectrum is known for each material. However, the surface reflectance at normal, R_{spec}, has been measured for many materials at many wavelengths, which prompts the approximation used in Eq. (3) [13].

To extend the BRDF model to model polarization, the $F_{\text{reflect},i}$ term becomes a vector with s- and p-components. If only linear vertical/horizontal polarization is considered, this vector has size 2×1. As this term is carried through the model, the terms $\rho_{\text{spec},i}$, $\rho_{\text{total},i}$, $F_{\text{sun},i}$, $F_{\text{obs},i}$ and m_{app} also become vectors. In the polarized form, Eq. (3) will become

$$\boldsymbol{F}_{\text{reflect},i} = \begin{bmatrix} R_s \\ R_p \end{bmatrix} \tag{23}$$

Equation (2) will now result in $\boldsymbol{\rho}_{\text{spec},i}$ being a vector. The diffuse reflection is assumed to be randomly polarized, so it is assumed to have an equal impact on each component. Therefore, Eq. (1) becomes

$$\boldsymbol{\rho}_{\text{total},i} = \begin{bmatrix} \rho_{\text{spec},s,i} + \rho_{\text{diff},i}/2 \\ \rho_{\text{spec},p,i} + \rho_{\text{diff},i}/2 \end{bmatrix} \tag{24}$$

The rest of the BRDF model can be proceeded through as written, replacing the scalars with the vector forms as necessary. Once $\boldsymbol{F}_{\text{obs},i}$ is computed, the Stokes vector can then be computed as

$$\boldsymbol{S} = \begin{bmatrix} F_{\text{obs},s} + F_{\text{obs},p} \\ F_{\text{obs},s} - F_{\text{obs},p} \end{bmatrix} \tag{25}$$

III. Surface Material Estimation

A. Surface Material Observability

Two parameters, the index of refraction m and the extinction coefficient k, define the surface materials. Since the polarized measurement provides two measurements, it is desired to check whether m and k are directly observable from the polarized measurements. The partials of a and b in Eq. (22) with respect to m and k are

$$\frac{\partial a}{\partial m} = \frac{m\left[p^{-1}(m^2+k^2-\sin^2\theta)+1\right]}{4\sqrt{p+m^2-k^2-\sin^2\theta}} \tag{26a}$$

$$\frac{\partial a}{\partial k} = \frac{k\left[p^{-1}(n^2+k^2-\sin^2\theta)-1\right]}{4\sqrt{p+m^2-k^2-\sin^2\theta}} \tag{26b}$$

$$\frac{\partial b}{\partial m} = \frac{m\left[p^{-1}(m^2+k^2-\sin^2\theta)-1\right]}{4\sqrt{p+m^2-k^2-\sin^2\theta}} \tag{26c}$$

$$\frac{\partial b}{\partial k} = \frac{k\left[p^{-1}(n^2+k^2-\sin^2\theta)+1\right]}{4\sqrt{p+n^2-k^2-\sin^2\theta}} \tag{26d}$$

where

$$p = \sqrt{(n^2-k^2-\sin^2\theta)^2+4n^2k^2)} \tag{27}$$

The partials of R_s and R_p with respect to a and b are

$$\frac{\partial R_s}{\partial a} = \frac{4\cos\theta(a^2-b^2-\cos^2\theta)}{(a^2+b^2+2a\cos\theta+\cos^2\theta)^2} \tag{28a}$$

$$\frac{\partial R_s}{\partial b} = \frac{8ab\cos\theta}{(a^2+b^2+2a\cos\theta+\cos^2\theta)^2} \tag{28b}$$

$$\frac{\partial R_p}{\partial a} = R_s\frac{4\sin\theta\tan\theta(a^2-b^2-\sin^2\theta\tan^2\theta)}{(a^2+b^2+2a\sin\theta\tan\theta+\sin^2\theta\tan^2\theta)^2} - \frac{\partial R_s}{\partial a}\frac{4a\sin\theta\tan\theta}{a^2+b^2+2a\sin\theta\tan\theta+\sin^2\theta\tan^2\theta} \tag{28c}$$

$$\frac{\partial R_p}{\partial b} = R_s\frac{8ab\sin\theta\tan\theta}{(a^2+b^2+2a\sin\theta\tan\theta+\sin^2\theta\tan^2\theta)^2} - \frac{\partial R_s}{\partial b}\frac{4a\sin\theta\tan\theta}{a^2+b^2+2a\sin\theta\tan\theta+\sin^2\theta\tan^2\theta} \tag{28d}$$

If m and k were observable from the Stokes vector, they must be observable from the Fresnel reflectance F_{reflect}. In this case, choosing F_{reflect} as the measurement from which to assess the observability allows the contributions of the facet orientations to be ignored. Then, the partials of the measurement with respect to m and k are given by the matrix

$$H = \begin{bmatrix} \frac{\partial R_s}{\partial a}\frac{\partial a}{\partial m}+\frac{\partial R_s}{\partial b}\frac{\partial b}{\partial m} & \frac{\partial R_s}{\partial a}\frac{\partial a}{\partial k}+\frac{\partial R_s}{\partial b}\frac{\partial b}{\partial k} \\ \frac{\partial R_p}{\partial a}\frac{\partial a}{\partial m}+\frac{\partial R_p}{\partial b}\frac{\partial b}{\partial m} & \frac{\partial R_p}{\partial a}\frac{\partial a}{\partial k}+\frac{\partial R_p}{\partial b}\frac{\partial b}{\partial k} \end{bmatrix} \tag{29}$$

It is found that $\text{rank}(H^T H) = 1$, so there does not exist direct observability of m and k. Therefore, m and k cannot be directly estimated in a filter. However, the inclusion of the S_1 Stokes parameter still provides information about m and k. This information is quantified as $\log(\det(H^T H))$ as in [1] and plotted against the angle θ in Fig. 3. It is noted that the valleys at $\pm\pi/2$ and 0 are actually asymptotic and would appear to approach negative infinity if θ were plotted with infinite resolution. This is because light reflected at $\theta = 0$ has no change to its polarization, and light reflected at $\theta = \pm\pi/2$ undergoes a $\pi/2$ rotation of the polarization. Since the incident light is unpolarized sunlight, both of these cases have $S_1 = 0$ and no information about m or k is contributed. It is seen that as the grazing incidence $\theta = \pm\pi$ is approached, the information gain increases.

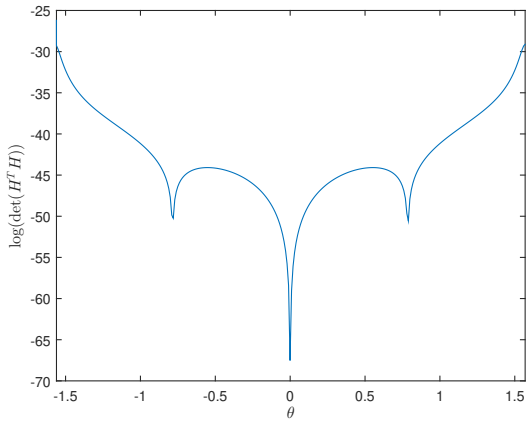

Fig. 3 Magnitude of information of m and k contributed by Stokes vector.

B. System Dynamics Model

A number of parameterizations exist to specify attitude, including Euler angles, quaternions, and Rodrigues parameters. Attitude dynamics in this paper use the quaternion, which is based on the Euler angle/axis parameterization. The quaternion is defined as $\boldsymbol{q} \equiv [\boldsymbol{\varrho}^T \quad q_4]^T$ with $\boldsymbol{\varrho} = \hat{\boldsymbol{e}} \sin(\nu/2)$, and $q_4 = \cos(\nu/2)$, where $\hat{\boldsymbol{e}}$ and ν are the Euler axis of rotation and rotation angle, respectively. The quaternion must satisfy a unit norm constraint $\boldsymbol{q}^T \boldsymbol{q} = 1$. The attitude matrix is given by

$$A(\boldsymbol{q}) = \Xi^T(\boldsymbol{q})\Psi(\boldsymbol{q}) \tag{30}$$

where

$$\Xi(\boldsymbol{q}) \equiv \begin{bmatrix} q_4 I_{3\times 3} + [\boldsymbol{\varrho}\times] \\ -\boldsymbol{\varrho}^T \end{bmatrix} \tag{31a}$$

$$\Psi(\boldsymbol{q}) \equiv \begin{bmatrix} q_4 I_{3\times 3} - [\boldsymbol{\varrho}\times] \\ -\boldsymbol{\varrho}^T \end{bmatrix} \tag{31b}$$

with $[\boldsymbol{g}\times]$ defined as the skew-symmetric cross product matrix such that $[\boldsymbol{g}\times]\boldsymbol{b} = \boldsymbol{g} \times \boldsymbol{b}$. The rotational dynamics are given by the coupled first-order differential equations:

$$\dot{\boldsymbol{q}}_I^B = \frac{1}{2}\Xi\left(\boldsymbol{q}_I^B\right)\omega_{B/I}^B \tag{32a}$$

$$\dot{\boldsymbol{\omega}}_{B/I}^B = J_{\text{RSO}}^{-1}\left(\boldsymbol{T}_{\text{ext}}^B - \left[\boldsymbol{\omega}_{B/I}^B\times\right] J_{\text{RSO}}\boldsymbol{\omega}_{B/I}^B\right) \tag{32b}$$

where $\boldsymbol{\omega}_{B/I}^B$ is the angular velocity of the RSO with respect to the inertial frame, expressed in body coordinates, J_{RSO} is the inertia matrix of the RSO, and $\boldsymbol{T}_{\text{ext}}$ is the net external torque action on the RSO, expressed in body coordinates.

C. Unscented Filtering Using Light Curve Data

An Unscented Kalman Filter (UKF) is used to estimate the rotational states as well as the projected area of the RSO from light curve data. The global parameterization of the attitude in the UKF is the quaternion, whereas a minimal parameterization involving the generalized Rodrigues parameters (GRPs) is used to define the local error [14]. Quaternions are the global parameterization of choice because their kinematics are free of singularities. The representation of the attitude error as a GRP is useful for the propagation and update steps of the attitude covariance because the structure of the UKF can be used direcly. A complete explanation of the quaternion and its mapping to GRPs is provided in [14].

Given a system model with initial state and covariance values, the UKF propagates the state vector and the error-covariance matrix recursively. At discrete observation times, the UKF updates the state and covariance matrix

conditioned on the information gained by the latest measurement. Discrete measurements are assumed to have the following form:

$$\tilde{\boldsymbol{y}}_k = \boldsymbol{h}\left(\boldsymbol{x}_k, t_k\right) + \boldsymbol{v}_k \tag{33}$$

where $\tilde{\boldsymbol{y}}_k$ is a measurement vector and $\boldsymbol{v}_k$ is the measurement noise, which is assumed to be a zero-mean Gaussian random variable with covariance $R_k \delta_{jk}$.

The UKF operates under the principle that (i) it is easier to propagate samples from a pdf through a general nonlinear function than to propagate the pdf itself and (ii) Gaussian distributions can be represented by a finite set of deterministically selected samples known as sigma points. Given an $L \times L$ error-covariance matrix P_k, the $2L + 1$ sigma points are constructed by

$$\boldsymbol{\sigma}_k \leftarrow 2L \text{ columns from } \pm\sqrt{(L+\lambda)P_k} \tag{34a}$$

$$\boldsymbol{\chi}_k(0) = \boldsymbol{\mu}_k \tag{34b}$$

$$\boldsymbol{\chi}_k(i) = \boldsymbol{\sigma}_k(i) + \boldsymbol{\mu}_k \tag{34c}$$

where $\sqrt{M}$ is shorthand notation for a matrix Z such that $M = Z\,Z^T$ and $\boldsymbol{\mu}_k$ is the mean of the distribution. Given that these points are selected to represent the distribution of the state vector, each sigma point is given a weight that preserves the information contained in the initial distribution:

$$W_0^{\text{mean}} = \frac{\lambda}{L+\lambda} \tag{35a}$$

$$W_0^{\text{cov}} = \frac{\lambda}{L+\lambda} + (1 - \alpha^2 + \beta) \tag{35b}$$

$$W_i^{\text{mean}} = W_i^{\text{cov}} = \frac{1}{2(L+\lambda)}, \quad i = 1, 2, \ldots, 2L \tag{35c}$$

where $\lambda = \alpha^2(L + \kappa) - L$ is a composite scaling parameter. The constant α controls the spread of the sigma point distribution and should be a small number $0 < \alpha \leq 1$, κ provides an extra degree of freedom that is used to fine-tune the higher-order moments, and β is used to incorporate prior knowledge of the distribution by weighting the mean sigma point in the covariance calculation. Typically $\beta = 2$ and $\kappa = 3 - L$ are good starting guesses for tuning the filter.

The reduced state vector for the joint attitude and area estimation problem is given by

$$\hat{\boldsymbol{x}}_k = \begin{bmatrix} \boldsymbol{\delta}\hat{\boldsymbol{p}}_k \\ \hat{\boldsymbol{\omega}}_k \\ \hat{\mathcal{A}} \end{bmatrix} \tag{36}$$

where $\boldsymbol{\delta}\hat{\boldsymbol{p}}$ is the error GRP state associated with the quaternion $\hat{\boldsymbol{q}}_I^B$ and $\hat{\cdot}$ is used to denote an estimate. Here it is noted that the subscript B/I and superscript B in $\boldsymbol{\omega}_{B/I}^B$ are omitted in this and the following sections for clarity. The initial estimate $\hat{\boldsymbol{x}}_0$ is the mean sigma point and is denoted $\boldsymbol{\chi}_0(0)$. The error GRP state of the initial estimate is set to zero, while the rest of the states are initialized by their respective initial estimates.

The attitude state errors are represented as error GRPs resulting in a minimum parameter representation for the attitude state error [15]. To within first order, the state error covariance of the attitude is invariant whether the errors are parameterized using quaternions or GRPs.. Therefore the attitude state error-covariance can be directly decomposed into error GRP sigma points for use in the UKF. The sigma points corresponding to the error GRPs are first converted into error quaternions so that the quaternion sigma points can be computed. The error quaternion, denoted by $\boldsymbol{\delta q}_k^-(i)$, associated with the i^{th} error GRP sigma point is computed by[15]

$$\boldsymbol{\delta \varrho}_k^-(i) = f^{-1}\left[a + \delta q_{4_k}^-(i)\right] \boldsymbol{\chi}_k^{\delta p}(i) \tag{37a}$$

$$\delta q_{4_k}^-(i) = \frac{-a||\boldsymbol{\chi}_k^{\delta p}(i)||^2 + f\sqrt{f^2 + (1-a^2)||\boldsymbol{\chi}_k^{\delta p}(i)||^2}}{f^2 + ||\boldsymbol{\chi}_k^{\delta p}(i)||^2} \tag{37b}$$

$$\boldsymbol{\delta q}_k^-(i) = \begin{bmatrix} \boldsymbol{\delta \varrho}_k^-(i) \\ \delta q_{4_k}^-(i) \end{bmatrix} \tag{37c}$$

where a is a parameter from 0 to 1 and f is a scale factor, which is often set to $f = 2(a+1)$ so that the attitude error covariance is that of the small roll, pitch and yaw angle errors. Here it is noted that the subscript I and superscript B in $\boldsymbol{q}_I^B$ and its estimates are omitted in this and the following sections for clarity. The i^{th} quaternion sigma point is given by a rotation of $\boldsymbol{\delta q}_k^-(i)$ about the *a priori* estimate:

$$\hat{\boldsymbol{q}}_k^-(i) = \boldsymbol{\delta q}_k^-(i) \otimes \hat{\boldsymbol{q}}_k^-(0) \tag{38}$$

where

$$\boldsymbol{q}' \otimes \boldsymbol{q} \equiv \begin{bmatrix} \Psi(\boldsymbol{q}') & \boldsymbol{q}' \end{bmatrix} \boldsymbol{q} \tag{39}$$

The sigma points are propagated through the system dynamics:

$$\dot{\boldsymbol{\chi}}(i) = \boldsymbol{f}\left(\boldsymbol{\chi}(i), \hat{\boldsymbol{q}}(i)\right) \tag{40}$$

where

$$\dot{\boldsymbol{\chi}}(i) = \boldsymbol{f}\left(\boldsymbol{\chi}(i), \hat{\boldsymbol{q}}(i)\right) \tag{41}$$

where

$$\boldsymbol{f}\left(\boldsymbol{\chi}, \hat{\boldsymbol{q}}\right) = \begin{bmatrix} \frac{1}{2}\Xi(\hat{\boldsymbol{q}})\hat{\boldsymbol{\omega}} \\ J_{\text{RSO}}^{-1}\left(\hat{\boldsymbol{T}}_{\text{ext}}^B - [\hat{\boldsymbol{\omega}}\times] J_{\text{RSO}}\hat{\boldsymbol{\omega}}\right) \\ 0 \end{bmatrix} \tag{42}$$

After propagation, the sigma points for the error GRP states are computed with the propagated attitude sigma points. The estimated mean sigma point quaternion, $\hat{\boldsymbol{q}}_{k+1}^-(0)$, is stored, and error quaternions corresponding to each propagated quaternion sigma point are computed as:

$$\boldsymbol{\delta}\hat{\boldsymbol{q}}_{k+1}^-(i) = \hat{\boldsymbol{q}}_{k+1}^-(i) \otimes \left[\hat{\boldsymbol{q}}_{k+1}^-(0)\right]^{-1} \tag{43}$$

where the notation for the conjugate quaternion is defined as:

$$\boldsymbol{q}^{-1} \equiv \begin{bmatrix} -\boldsymbol{\varrho} \\ q_4 \end{bmatrix} \tag{44}$$

Using the result of Eq. (43), the error GRP sigma points are computed as

$$\boldsymbol{\delta p}_{k+1}^-(i) = f\frac{\boldsymbol{\delta}\hat{\boldsymbol{\varrho}}_{k+1}^-(i)}{a + \delta\hat{q}_{4_{k+1}}^-(i)} \tag{45}$$

After setting the error GRP for the mean sigma point to zero, the propagated sigma points are reconstructed. The propagated mean and covariance are calculated as a weighted sum of the sigma points as

$$\hat{\boldsymbol{x}}_{k+1}^- = \sum_{i=0}^{2L} W_i^{\text{mean}}\, \boldsymbol{\chi}_{k+1}(i) \tag{46a}$$

$$P_{k+1}^- = \sum_{i=0}^{2L} W_i^{\text{cov}} \left[\boldsymbol{\chi}_{k+1}(i) - \hat{\boldsymbol{x}}_{k+1}^-\right]\left[\boldsymbol{\chi}_{k+1}(i) - \hat{\boldsymbol{x}}_{k+1}^-\right]^T + Q_{k+1} \tag{46b}$$

where Q_{k+1} is the discrete-time process noise covariance.

The measurements are taken to be the Stokes vector, which is limited to the nonzero (S_0 and S_1) parameters, hence

$$\tilde{\boldsymbol{y}}_k = \begin{bmatrix} \hat{S}_0 \\ \hat{S}_1 \end{bmatrix} \tag{47}$$

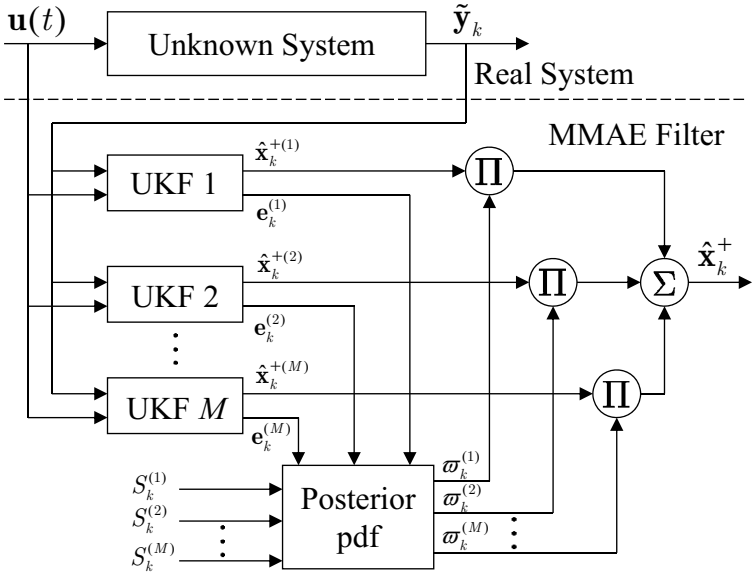

Fig. 4 MMAE process.

D. Material Estimation using Multiple-Model Adaptive Estimation

Although the parameters n and k cannot be estimated directly in a filter, an MMAE approach using a bank of materials can be used to identify the material. In this approach, the UKFs described in the previous section are used to estimate the attitude and the area of the object.

MMAE is a recursive algorithm that uses a bank of estimators, each dependent on a particular hypothesis, to determina an estimate based upon an unknown physical process under consideration. In particular, the hypotheses can correspond to different mathematical models of the same physical process or of the same model but dependent upon different constants or model parameters. The basic framework of MMAE can be seen in Fig. 4.

A finite set of hypothesis $\{\boldsymbol{p}^{(\ell)};\ \ell = 1, \ldots, M\}$ are used to seed the bank of estimators. The finite set of parameters can be the results of discretizing a continuous parameters space or describe a discrete parameter space of interest. The goal of the estimation process is to determine the conditional pdf of the ℓ^{th} hypothesis, $\boldsymbol{p}^{(\ell)}$, given all the measurements. Application of Bayes' rule yields

$$p\left(\boldsymbol{p}^{(\ell)}|\tilde{\boldsymbol{Y}}_k\right) = \frac{p\left(\tilde{\boldsymbol{Y}}_k|\boldsymbol{p}^{(\ell)}\right) p\left(\boldsymbol{p}^{(\ell)}\right)}{\sum_{j=1}^{M} p\left(\tilde{\boldsymbol{Y}}_k|\boldsymbol{p}^{(j)}\right) p\left(\boldsymbol{p}^{(j)}\right)} \tag{48}$$

where $\tilde{\boldsymbol{Y}}_k$ denotes the sequence $\{\tilde{\boldsymbol{y}}_0,\ \tilde{\boldsymbol{y}}_1,\ \ldots,\ \tilde{\boldsymbol{y}}_k\}$. The *a posteriori* probabilities can be computed through[16]

$$\begin{aligned} p\left(\boldsymbol{p}^{(\ell)}|\tilde{\boldsymbol{Y}}_k\right) &= \frac{p\left(\tilde{\boldsymbol{y}}_k,\ \boldsymbol{p}^{(\ell)}|\tilde{\boldsymbol{Y}}_{k-1}\right)}{p\left(\tilde{\boldsymbol{y}}_k|\tilde{\boldsymbol{Y}}_{k-1}\right)} \\ &= \frac{p\left(\tilde{\boldsymbol{y}}_k|\hat{\boldsymbol{x}}_k^{-(\ell)}\right) p\left(\boldsymbol{p}^{(\ell)}|\tilde{\boldsymbol{Y}}_{k-1}\right)}{\sum_{j=1}^{M}\left[p\left(\tilde{\boldsymbol{Y}}_k|\hat{\boldsymbol{x}}_k^{-(j)}\right) p\left(\boldsymbol{p}^{(j)}|\tilde{\boldsymbol{Y}}_{k-1}\right)\right]} \end{aligned} \tag{49}$$

The conditional probabilities of the observations based on each hypothesis (likelihood), $p\left(\tilde{\boldsymbol{y}}_k|\hat{\boldsymbol{x}}_k^{-(\ell)}\right)$, are given as

$$p\left(\tilde{\boldsymbol{y}}_k|\hat{\boldsymbol{x}}_k^{-(\ell)}\right) = \frac{1}{\det\left(2\pi S_k^{(\ell)}\right)^{1/2}} \exp\left\{-\frac{1}{2}\boldsymbol{e}_k^{(\ell)T} S_k^{(\ell)^{-1}} \boldsymbol{e}_k^{(\ell)}\right\} \tag{50}$$

where measurement residual for the ℓ^{th} hypothesis is given by

$$\boldsymbol{e}_k^{(\ell)} = \tilde{\boldsymbol{y}}_k - \hat{\boldsymbol{y}}_k^{-(\ell)} \tag{51}$$

and corresponding residual covariance matrix from the UKF is

$$S_k^{(\ell)} = P_k^{vv} \tag{52}$$

where P_k^{vv} is the innovations covariance using the ℓ^{th} filter.

Note that the denominator of Eq. (49) is just a normalizing factor to ensure that $p\left(\boldsymbol{p}^{(\ell)}|\tilde{\boldsymbol{Y}}_k\right)$ is a pdf. Equation (49) can now be recast as a recursion formula to define the MMAE weights $\varpi_k^{(\ell)}$ as

$$\begin{aligned} \varpi_k^{(\ell)} &= \varpi_{k-1}^{(\ell)} p\left(\tilde{\boldsymbol{y}}_{k-1}|\hat{\boldsymbol{x}}_{k-1}^{-(\ell)}\right) \\ \varpi_k^{(\ell)} &\leftarrow \frac{\varpi_k^{(\ell)}}{\sum_{j=1}^{M} \varpi_k^{(j)}} \end{aligned} \tag{53}$$

where $\varpi_k^{(\ell)} \equiv p\left(\boldsymbol{p}^{(\ell)}|\tilde{\boldsymbol{y}}_k\right)$. Note that only the current time likelihood function is needed to update the weights. The weights at time t_0 are initialized to $\varpi_0^{(\ell)} = 1/M \;\forall\; \ell$. The convergence properties of MMAE are shown in Ref. 17, which assumes ergodicity in the proof. The ergodicity assumptions can be relaxed to asymptotic stationarity and other assumptions are even possible for non-stationary situations.

From Eq. (53) and Eq. (50) it is seen that hypotheses having lower residuals will have probabilities that will increase with time; this will favor hypotheses that fit the observations better. Also from Eq. (50) it is seen that hypotheses which have small values for $\det(S_k^{(\ell)})$ will have probabilities that will grow. Assuming that all filters have same measurement noise covariance matrix R_k, this will favor hypotheses that have smaller variance. Therefore the MMAE process will tend to select the minimum variance hypothesis from the set of hypotheses.

E. Results

MMAE is run with a bank of materials as listed in Table 1. The true material has been simulated to be aluminum. A

Table 1 Material bank

Material	m	k
Aluminum	1.1987	7.0488
Gold	0.2773	2.9278
Copper	0.6366	2.7834
Nickel	1.9648	3.8352
Tin	2.1600	6.3500
Titanium	2.9300	3.9850
Glass	1.5123	0
Polymide	1.4950	0
Gallium Arsenide	3.8570	0.1980

rotational rate of $\omega_0 = [-0.0012 \quad 0.0005 \quad 0.0008]^T$ rad/s is simulated. The MMAE weights are initialized to be equal. It is assumed that the total brightness S_0 can be measured to one-tenth magnitude and the polarization parameter S_1 can be measured to milli-magnitude. This is based on a measurement from a polarimeter, where the accuracy of relative measurements between adjacent pixels is greater than the absolute accuracy relative to the true intensity of the light entering the sensor.

Figure 5 shows the MMAE weights over time. It is seen that after the first large glint event, the MMAE weight of the correct material goes to 1. Glint events are required to correctly identify the material as they are the periods when there is substantial specular reflection. Since only specular reflection contains meaningful polarization data, diffuse

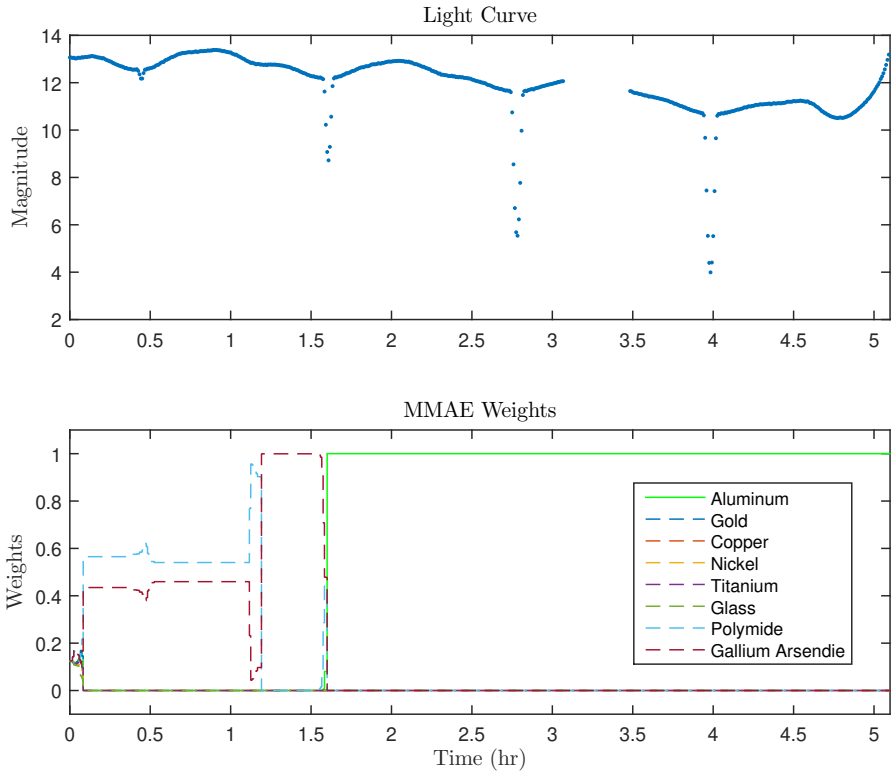

Fig. 5 MMAE weights for material estimation.

reflection does not aid in the material identification. Unpolarized data is not sufficient to identify the material, as even though there is a dependency on reflectance in the overall brightness, the UKF will simply increase the area $\mathcal{A}$ for a less-reflective surface. The addition of the polarization information is independent of this relationship and can be used to correctly identify the material. Figure 6 shows the estimation of the area for the filter corresponding to aluminum, the correct material.

IV. Conclusion

Polarized light has been demonstrated to allow for material identification of a space object from light curves. This occurs because specular reflectance of unpolarized light is polarized. The amount of polarization in the specular reflection is dependent on the degree of polarization, which is dependent on the index of refraction and extinction coefficient, which are properties of the surface materials. Diffuse reflections are randomly polarized and thus do not contribute to the polarization of the reflection. For a single-material object, material identification has been demonstrated after one significant glint event using only a monochromatic light curve. This effectiveness of this method could be increased when coupled with multispectral imaging. Future work involves estimating material abundances for objects made of multiple materials and assessing the impact of this method on multispectral material identification methods.

References

[1] Hinks, J., Linares, R., and Crassidis, J., "Attitude Observability from Light Curve Measurements," *AIAA Guidance, Navigation, and Control Conference*, AIAA, Reston, VA, 2013. doi:10.2514/6.2013-5005.

[2] Wetterer, C. J., and Jah, M., "Attitude Estimation from Light Curves," *Journal of Guidance, Control and Dynamics*, Vol. 32, No. 5, 2009, pp. 1648–1651. doi:10.2514/1.44254.

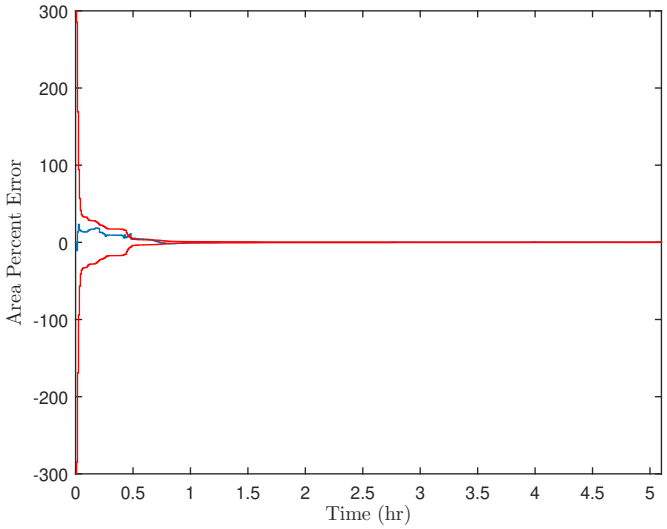

Fig. 6 Area estimate for filter assuming aluminum.

[3] Linares, R., Jah, M. K., Crassidis, J. L., and Nebelecky, C. K., "Space Object Shape Characterization and Tracking Using Light Curve and Angles Data," *Journal of Guidance, Control, and Dynamics*, Vol. 37, No. 1, 2014, pp. 13–25. doi:10.2514/1.62986.

[4] Wetterer, C. J., Hunt, B., Hamada, C., Crassidis, J. L., and Kervin, P., "Shape, Surface Parameter, and Attitude Profile Estimation Using a Multiple Hypothesis Unscented Kalman Filter," *AAS/AIAA Space Flight Mechanics Meeting*, AAS, Springfield, VA, 2014. AAS Paper #14-303.

[5] Wetterer, C. J., Chow, C. C., Crassidis, J. L., and Linares, R., "Simultaneous Position Velocity, Attitude, Angular Rates, and Surface Parameter Estimation Using Astrometric and Photometric Observations," *16th International Conference on Information Fusion*, IEEE, Piscataway, NJ, 2013, pp. 997–1004. doi:10.2514/6.2013-5005.

[6] Linares, R., Jah, M., Crassidis, J., Leve, F., and Kelecy, T., "Astrometric and Photometric Data Fusion for Inactive Space Object Mass and Area Estimation," *Acta Astronautica*, Vol. 99, 2014, pp. 1–15. doi:10.1016/j.actaastro.2013.10.018.

[7] Hall, D., Hamada, K., Kelecy, T., and Kervin, P., "Surface Material Characterization from Non-Resolved Multi-Band Optical Observations," *Advanced Maui Optical Space Surveillance Technologies Conference*, 2012.

[8] Stryjewski, J., Hand, D., Tyler, D., Murali, S., Roggemann, M., and Peterson, N., "Real Time Polarization Light Curves for Space Debris and Satellites," *Advanced Maui Optical and Space Surveillance Technologies Conference*, 2010.

[9] Schott, J., *Fundamentals of Polarimetric Remote Sensing*, Society of Photo-Optical Instrumentation Engineers, 2009.

[10] Ashikmin, M., and Shirley, P., "An Anisotropic Phong Light Reflection Model," Tech. rep., University of Utah, Salt Lake City, UT, 2000.

[11] Markley, F. L., and Crassidis, J. L., *Fundamentals of Spacecraft Attitude Dynamics and Control*, Springer, New York, NY, 2014, Chap. 6, pp. 71, 143–147, 242–244, 258.

[12] Shirley, P., "Physically Based Lighting Calculations for Computer Graphics," Ph.D. thesis, University of Illinois at Urbana-Champaign, 1991.

[13] Schlick, C., "An Inexpensive BRDF Model for Physically-based Rendering," *Computer Graphics Forum*, Vol. 13, 1998. doi:10.1111/1467-8659.1330233.

[14] Schaub, H., and Junkins, J., "Stereographic Orientation Parameters for Attitude Dynamics: A Generalization of the Rodrigues Paramaters," *Journal of the Astronautical Sciences*, Vol. 4, No. 1, 1996, pp. 1–20.

[15] Crassidis, J., and Markley, F., "Unscented Filtering for Spacecraft Attitude Estimation," *Journal of Guidance, Control, and Dynamics*, Vol. 26, No. 4, 2003, pp. 536–542. doi:10.2514/2.5102.

[16] Crassidis, J. L., and Junkins, J. L., *Optimal Estimation of Dynamic Systems*, 2nd ed., Chapman & Hall/CRC, Boca Raton, FL, 2012, pp. 463–465. doi:10.2514/1.J052115.

[17] Anderson, B., and Moore, J., *Optimal Filtering*, Dover, New York, 2005.